Nanoscale

PAPER

View Article Online
View Journal | View Issue

Cite this: *Nanoscale*, 2026, **18**, 298

Scalable synthesis of spatially confined Ge quantum dots with tunable quantum confinement

Su Hyun Park, Gyeong Min Seo, Jeong Wook Kim, Yun Ho Lee, Gyubin Lee, Hong Jae Lee and Byoung Don Kong *

We report a scalable, thermodynamically guided method for synthesizing germanium quantum dots embedded in a silicon oxide matrix with nanometer-scale precision. By engineering the oxidation and annealing conditions of silicon–germanium alloy layers, we achieved spatially confined, crystalline germanium quantum dots as small as 9.2 nanometers with tunneling oxide thicknesses down to 3.2 nanometers—suitable for room-temperature quantum confinement. Molecular dynamics simulations across a range of germanium compositions predict the agglomeration behaviour and size evolution of the quantum dots, while an analytical model enables predictive tuning of quantum dot dimensions and oxide thickness based on their initial alloy composition. Experimental validation using scanning transmission electron microscopy, X-ray diffraction, and photoluminescence spectroscopy confirms crystallinity and size-dependent optical emission in the visible range. In contrast to earlier nanocrystal memory systems that relied on randomly distributed germanium precipitates embedded deep in thick oxides, our method enables precise formation of shallow, single-layer quantum dots with controlled geometry. These findings establish a robust platform for room-temperature quantum dot electronics, combining tunable confinement and compatibility with integrated circuit architectures.

Received 8th October 2025,
Accepted 20th November 2025

DOI: 10.1039/d5nr04252f

rsc.li/nanoscale

1 Introduction

Semiconductor quantum dots (QDs), owing to their discrete energy levels and tunable quantum properties, underpin many of today's most promising advances in quantum materials and nanodevices.[1] Since the pioneering work of Louis Brus—who first demonstrated that the electronic structure of nanocrystals could be tailored by size[2]—colloidal and solid-state QDs have enabled a wide spectrum of technologies, from light-emitting devices to memory and sensing platforms. In contrast to potential-well-based systems that often require cryogenic operation, nanocrystal-based QDs offer robust quantum confinement even at room temperature, making them particularly attractive for scalable quantum electronics.[3–8]

In solid-state systems, Ge nanocrystals spontaneously form in oxide matrices such as SiGeO during thermal processing. This phenomenon was originally discovered not in the pursuit of quantum control, but in the context of CMOS device fabrication, where Ge aggregation during SiGe oxidation complicated the formation of uniform gate dielectrics.[9,10] Later, researchers repurposed this self-assembly behaviour for nonvolatile memory,[11–14] emphasizing charge retention over control of size, position, or interface proximity. These early systems featured randomly distributed Ge precipitates, often embedded deep within thick oxide layers, and lacked the confinement precision required for fast, low-voltage quantum operations.[15–18]

The formation of Ge nanostructures through oxidation of SiGe alloys has been previously reported.[19–21] In these earlier studies, polycrystalline SiGe layers embedded between oxides were oxidized, and Ge nanocrystals were formed within the oxide matrix during annealing steps. In contrast, our approach is designed to generate a single, spatially uniform layer of Ge QDs from a single SiGe layer directly on the Si substrate. The low temperature oxidation step is first used to convert the SiGe film into a homogeneous SiGeO layer while preserving a high-quality interface between SiGe and the oxide. Subsequent high temperature annealing then drives the self-limited condensation of Ge atoms into uniformly sized QDs. While both Si and Ge are oxidized at low temperatures, elevated annealing temperatures promote dissociation of Ge–O bonds, which are considerably less thermodynamically stable than Si–O bonds, thereby facilitating the precipitation of elemental Ge.[16,22,23]

Here, we advance this concept by demonstrating a deterministic, self-assembly-based strategy for producing spatially confined, crystalline Ge QDs within a SiO_x matrix, positioned within 3.2 nm of the semiconductor interface. By carefully engineering the oxidation and double-step annealing of SiGe

Department of Electrical Engineering, Pohang University of Science and Technology (POSTECH), Pohang 37673, Korea. E-mail: bdkong@postech.ac.kr

alloy layers, sub-10 nm Ge QDs are synthesized in a single plane, enabling tunable quantum confinement. The synthesis pathway is guided by molecular dynamics (MD) simulations and analytical modelling, allowing predictive design of QD size and tunnelling oxide thickness from the initial composition. Structural and photoluminescence characterization confirm quantum confinement effects at room temperature. The proposed synthesis method offers a practical and scalable approach for synthesizing Ge nanocrystal quantum dots (NCQDs) compatible with conventional Si-based technology. This work not only advances the understanding of selective oxidation and self-assembly mechanisms in the Si–Ge–O system but also provides a versatile platform for the fabrication of next-generation QD devices with broad applications in optoelectronics, memory, and sensing technologies.

2 Results and discussion

2.1 Ge quantum dot formation within oxides

The formation of Ge NCQDs was achieved by controlling the oxidation-driven transformation of the SiGe layer and subsequent thermal annealing. At oxidation temperatures below 600 °C, the activation energy for germanium diffusion exceeds the available thermal energy, leading to the formation of a homogeneous SiGeO alloy as both silicon and germanium are oxidized. Upon subsequent annealing at temperatures above 600 °C, the mobility of germanium atoms increases, enabling their diffusion and agglomeration. Due to the large thermodynamic stability difference between silicon dioxide and germanium dioxide as described by the Gibbs triangle of the Si–Ge–O system,[24,25] elemental germanium becomes the energetically preferred phase, leading to the precipitation of crystalline nanodots.

The initial oxidation process differs from conventional thermal oxidation of silicon wafers; it employs a very low oxygen flow to form a precisely controlled nanometer-scale SiGeO alloy. As illustrated in Fig. 1, the process begins with the deposition of a Si_xGe_{1-x} film by molecular beam epitaxy (MBE) or ultra-high vacuum chemical vapor deposition (UHV-CVD), ensuring compatibility with standard silicon processing. Thermal oxidation was performed at 550–600 °C in a tube furnace under near-atmospheric pressure (770 Torr) with pure O_2 gas supplied at 20 sccm. In this low temperature regime, the diffusivities of Si and Ge decrease more sharply than the oxidation rate, allowing both elements to oxidize and form a homogeneous amorphous SiGeO alloy layer. By adjusting the oxidation duration, the thickness and composition of this intermediate layer can be precisely controlled.

To suppress further oxygen ingress during subsequent annealing, which may increase the thickness, a SiN capping layer was deposited by plasma-enhanced chemical vapor deposition (PECVD). Actually, any dense material that can block the oxygen passage would serve for this, and indeed, for certain samples prepared for X-ray diffraction (XRD), a TiN layer was first deposited *via* atomic layer deposition (ALD), followed by the same SiN capping process.

Post-oxidation, Ge NCQDs were formed through rapid thermal annealing (RTA) in nitrogen. Before annealing, the chamber was evacuated to $\sim 1 \times 10^{-3}$ Torr and then backfilled with N_2 to $\sim 1 \times 10^{-1}$ Torr. Two RTA strategies were employed: (1) single-step annealing at 800 °C and (2) double-step annealing consisting of an initial high-temperature pulse at 1000 °C followed by a lower-temperature step at 700–800 °C. According to the previous studies,[15] the reduction of GeO_x is more promoted at higher temperature annealing, enabling the initial formation of Ge nanoparticles. As GeO_x defects are reduced during the first annealing at 1000 °C, the subsequent growth of Ge QDs occurs with improved size uniformity and spatial distribution within the oxide matrix. Furthermore, the vacuum conditions and pure N_2 ambient conditions prevented re-oxidation of Ge, facilitating phase-pure NCQD growth.

A critical feature of this method is the ability to control the vertical position of the Ge QDs and the surrounding oxide thickness by adjusting the thickness and composition of the SiGeO alloy. In our process, the SiGe layer is directly oxidized at low temperature, deliberately forming a homogeneous SiGeO alloy. After depositing a SiN capping layer, high temperature annealing drives Ge extraction from the SiGeO alloy. Importantly, this approach obviates the need for a separate tunnelling oxide growth step; an ultrathin tunnelling oxide forms spontaneously as the remaining SiGeO is converted to SiO_2 during the annealing process.

Controlling the oxidation time and the initial SiGe composition enables deterministic control over the final QD size and oxide thickness, as it dictates the absolute amount of available germanium for aggregation. Moreover, compared to ion implantation methods, which typically introduce germanium at concentrations below 10^{19} cm^{-3}, this SiGe oxidation strategy offers much higher atomic densities (up to 10^{22} cm^{-3}) and superior control over depth and spatial confinement. Achieving nanometer-scale vertical accuracy using ion implan-

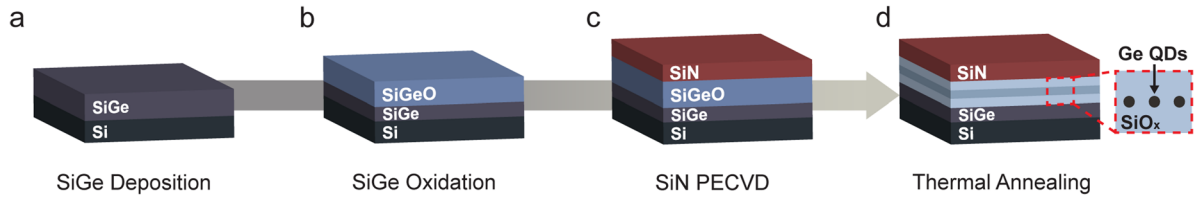

Fig. 1 (a–d) Schematic overview of the Ge QD synthesis process. This process was followed in the experiments.

tation remains highly challenging, while our method enables intrinsic alignment near the channel region with sub-5 nm oxide encapsulation.

The formation of Ge NCQDs and their crystallinity were confirmed through structural and optical characterization. Cross-sectional scanning transmission electron microscopy (STEM) and X-ray diffraction (XRD) measurements were performed. The STEM imaging of single-step annealed samples (800 °C, 30 minutes) revealed Ge NCQDs with a rather broad spatial distribution. The average diameter turned out to be 3.7 nm, and the total oxide thickness was ~12.0 nm (Fig. 3(b)).

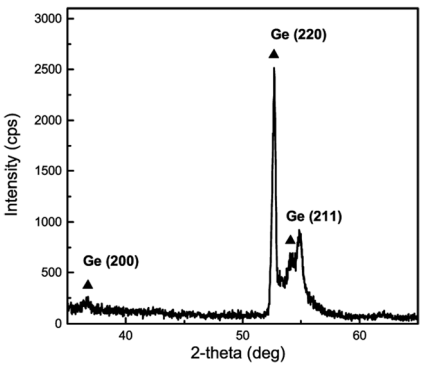

Fig. 2 XRD pattern of Ge QDs with a single-step annealing process.

XRD results (Fig. 2) confirmed crystallinity with Bragg peaks corresponding to Ge(220) planes. The Ge(220) peak exhibited a full width at half maximum (FWHM) of 0.279°, further validating nanocrystal formation. Weak peaks at Ge(200) and (211) were also observed, which can be attributed to truncation effects and structural disorders arising from the nanoscale QD size.[26,27]

The double-step annealing process appears to be more suitable to achieve improved spatial confinement for the controlled formation of QD arrays. For the double-step annealing process, the samples were first annealed at 1000 °C for 5 minutes, followed by a second step at 700 °C for 1 minute. This strategy leverages the enhanced mobility and reduction of GeO_x at high temperature to seed NCQD formation, while the second step stabilizes the growth and improves uniformity. As shown in Fig. 3(d), this method yielded a single row of Ge NCQDs embedded in a 17.8 nm-thick oxide layer, with QD diameters of ~9.2 nm and tunnelling oxide thickness as low as 3.2 nm. From the energy-dispersive spectroscopy (EDS) mapping in Fig. 4, a nicely formed single layer of QDs with an even spatial distribution can be clearly identified. The QDs are distinctly represented by the red colour, with the corresponding vacancies observed in the elemental maps of other atoms.

Temperature control, for example during the low temperature Si–Ge–O matrix formation and successive annealing, appeared to be critical. The temperature-dependent oxidation

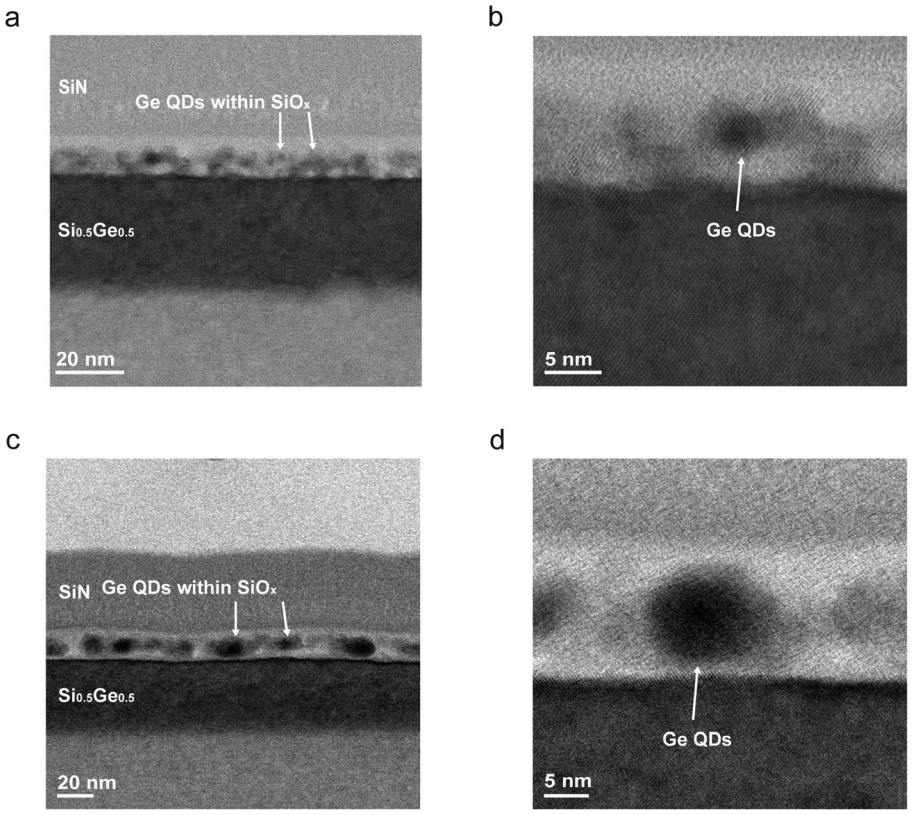

Fig. 3 Bright field STEM images of Ge NCQDs embedded in the oxide after (a and b) single-step annealing and (c and d) double-step annealing.

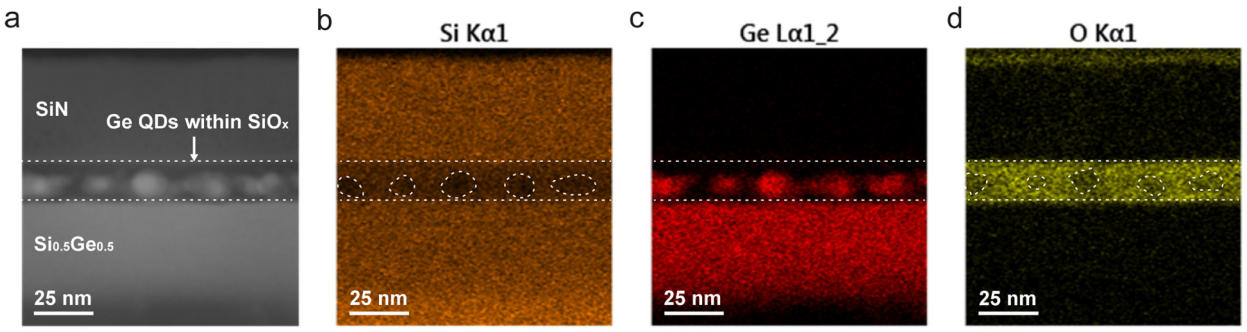

Fig. 4 EDS maps of the sample after double-step annealing. (a) Dark field STEM image. (b–d) Elemental distribution maps of Si, Ge and O corresponding to the STEM image.

behaviour of SiGe/Si layers was experimentally investigated at two different temperatures (600 °C and 850 °C) under near-atmospheric conditions, as detailed in the SI. At 850 °C, preferential oxidation of Si leads to Ge accumulation and the formation of a Ge-rich layer (GRL) near the SiO_2/SiGe interface (SI Fig. S3). In contrast, at 600 °C both Si and Ge oxidize, supporting SiGeO alloy formation. These observations align with prior thermodynamic studies and confirm the dual role of low temperature oxidation and high temperature annealing in producing confined crystalline Ge NCQDs. Consequently, the temperature-dependent behaviour of the Si–Ge–O system directly contributed to the formation of a single row of Ge NCQDs through the double-step annealing process.

2.2 Optical evidence of quantum confinement

Optical properties were evaluated through photoluminescence (PL) spectroscopy, revealing discrete visible-light emission consistent with quantum confinement.[28] A total of nine samples were prepared from three types of $Si_{1-x}Ge_x$/Si layers with different Ge contents (x = 0.20, 0.33, and 0.50). For each composition, annealing durations of 20, 30, and 40 minutes were applied under 800 °C single-step RTA, yielding samples labelled A_{1-3} (x = 0.20), B_{1-3} (x = 0.33), and C_{1-3} (x = 0.50). PL spectra were measured at room temperature under laser excitation ranging from 300 to 650 nm. Among these, distinct emission peaks were most clearly observed under 300 nm excitation. As shown in Fig. 5(a–c) and summarized in Table 1, the PL emission exhibited a strong dependence on both the annealing time and Ge content. With increased annealing duration, five distinct peaks (labelled a–e) became progressively sharper and more separated, indicating improved NCQD size uniformity and enhanced thermodynamic stability. The highest intensity peak (b), observed in the C_3 sample (x = 0.50, 40 minutes), was centered at 2.568 eV with a FWHM of 0.234 eV. From the Brus equation,[29,30] this corresponds to a QD radius of ~2.6 nm and a size variation of ΔR ~0.1 nm, where R is the radius of QDs. ΔR can be considered as a size disorder in the system. These values exhibited an excellent agreement with the average QD size of 5.2 nm observed in the STEM image of sample C_3 (SI Fig. S4(c)). While there were possibilities of the peaks originating from the optical resonance such as Fabry–Pérot resonance due to the SiN_x capping layer, we excluded this possibility for two reasons. Firstly, the resonance peak period differed from the value estimated from the SiN_x thickness, and secondly, the peak did not appear in other longer-wavelength regions, while there must have been some signature if it were a purely optical phenomenon. Considering the beam spot size of at least a few mm^2 in the PL measurement, this indicates the reasonable uniformity in QD sizes.

It is worth noting that even QDs of the same nominal size may differ structurally. For example, small aggregates of Au or Pt atoms can exhibit confinement-like effects without crystallinity. However, such non-crystalline clusters would not behave as semiconductor QDs: their discretized levels would be much smaller, requiring much smaller sizes to account for the observed PL range. In contrast, the agreement of our PL spectra with the Brus formula, which assumes semiconductor effective masses derived from a periodic lattice, indicates that the Ge QDs here are at least partially crystalline. With respect to defects, only states within the band gap can contribute to PL, while states inside the bands are filled and inactive. The discrete energy levels we observed were much larger than typical defect-related energies, and no sub-gap peaks were detected, making it unlikely that intrinsic defect states are involved. One might also consider defect states in the Si or SiGe substrates; however, since both are indirect band gap materials and the observed PL emission is above 2 eV, it is unlikely that substrate-related defects contribute to the measured spectra.

A clear redshift in PL emission was observed with increasing Ge content—from $Si_{0.8}Ge_{0.2}$ to $Si_{0.5}Ge_{0.5}$—consistent with quantum confinement behaviour (Fig. 5(d)). As the Ge supply in the Si–Ge–O matrices increases, the QD size increases, and the effective bandgap narrows, leading to lower-energy emission.[31] Based on the PL peak positions presented in Table 1, the estimated QD diameters ranged from ~4 nm to ~6 nm across all sample sets. The emission wavelengths, spanning 358–550 nm, demonstrate tunability within the visible spectrum through control of Ge content and annealing time.

These results underscore the role of annealing in achieving size-controlled QD formation. While 30 minutes of annealing was sufficient to produce crystalline Ge QDs, extending to

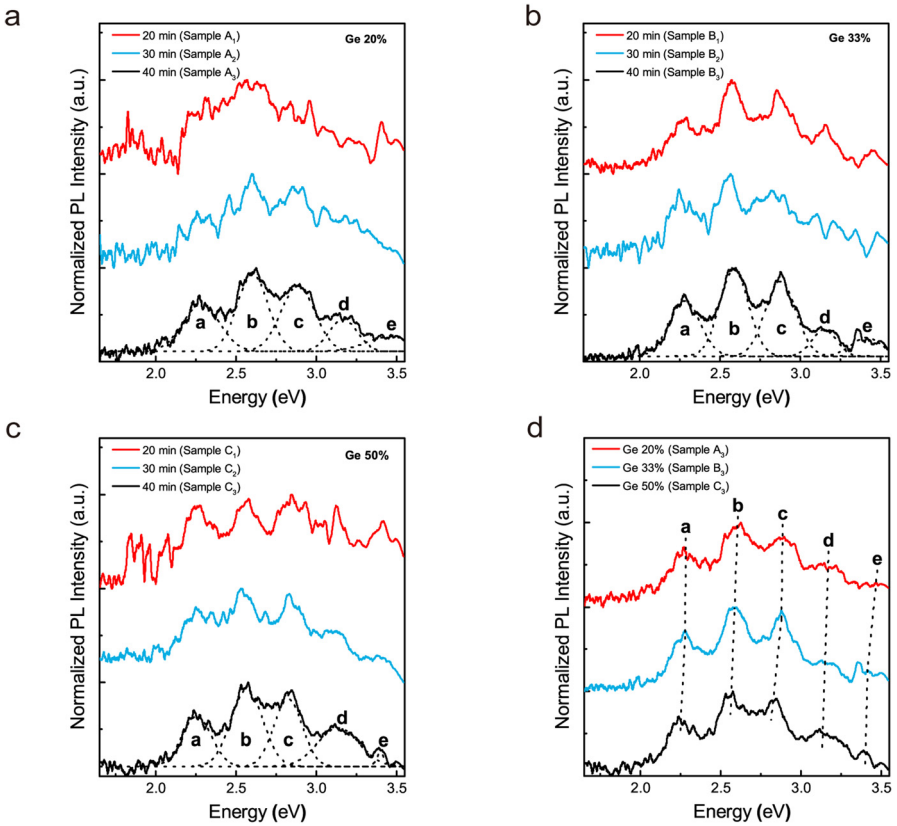

Fig. 5 (a–c) Normalized PL spectra of 9 samples at 300 nm (4.13 eV) excitation energy. The Ge concentrations in the $Si_{1-x}Ge_x$ layers used for Ge QD formation vary by 20%, 33%, and 50%, corresponding to samples A_{1-3}, samples B_{1-3}, and samples C_{1-3}. In each sample group (A, B, and C), the Ge QD growth times were controlled in 10-minute intervals. The sample numbers 1–3 correspond to growth times of 20, 30, and 40 minutes, respectively. Deconvolution analysis of the PL spectra at samples of 40 minutes was performed, with the resulting PL peaks marked as a, b, c, d, and e. (d) Normalized PL spectra of sample A_3, sample B_3, and sample C_3. The Ge QD growth time was 40 minutes. Dotted black lines indicate the shifts of each PL peak.

Table 1 The positions of the PL peaks and FWHM properties for samples A_3, B_3, and C_3 with a Ge QD growth time of 40 minutes

	Sample A_3		Sample B_3		Sample C_3	
	Peak (eV)	FWHM (eV)	Peak (eV)	FWHM (eV)	Peak (eV)	FWHM (eV)
a	2.283 ± 0.0015	0.271	2.281 ± 0.0008	0.226	2.255 ± 0.0011	0.216
b	2.604 ± 0.0015	0.227	2.588 ± 0.0007	0.212	2.568 ± 0.0014	0.234
c	2.885 ± 0.0016	0.251	2.877 ± 0.0009	0.224	2.824 ± 0.0015	0.207
d	3.167 ± 0.0045	0.207	3.149 ± 0.0025	0.179	3.138 ± 0.0027	0.304
e	3.466 ± 0.0137	0.361	3.412 ± 0.0038	0.222	3.400 ± 0.0021	0.059

40 minutes yielded narrower and more reproducible PL peaks, indicating better size distribution and thermal stabilization. Collectively, the structural and optical data confirm that the Ge NCQDs exhibit pronounced quantum confinement effects and tunable optical properties at room temperature, positioning them as promising building blocks for integrated optoelectronic and quantum devices.

2.3 Modelling and predictive control of quantum dot size and distribution

To understand and predict the formation of Ge NCQDs within a SiO_x matrix, MD simulations using the Large-scale Atomic/Molecular Massively Parallel Simulator (LAMMPS) were conducted.[32] The MD study provides cost-effective versatility that can supplement the experiments to obtain enough data to postulate a predictive QD formation modelling. A Tersoff potential was employed to model the Si–Ge–O ternary system (details are provided in the SI). The simulations began with a base amorphous SiO_2 structure containing 4096 Si atoms and 8192 O atoms. Ge atoms were introduced by substituting Si atoms at various concentrations, yielding five alloy models with Ge contents of 10%, 20%, 30%, 40%, and 50%. Each simulation cell measured 5.70 nm × 5.70 nm × 5.70 nm with periodic boundary conditions in all directions.

The samples were thermally annealed at 3000 K using an isothermal–isobaric (NPT) ensemble, a temperature below the melting point of Ge.[33] Although this temperature exceeds realistic processing conditions, such elevated values are commonly used in MD simulations to accelerate atomic diffusion within computationally tractable timescales. Temperature and pressure were controlled *via* a Nosé–Hoover thermostat and barostat with damping constants of 100 and 1000, respectively, and a 1 fs timestep was used throughout.

After 100 ns of simulated annealing, the formation of nearly spherical Ge clusters in samples was observed with up to 30% Ge content (Fig. 6(f–h)). In the 30% Ge sample, a single Ge NCQD was clearly resolved. For samples with 40% and 50% Ge (Fig. 6(i and j)), partial agglomeration occurred, but additional annealing would be required to achieve full spherical confinement. As shown in Fig. 6(k–o), partial radial distribution functions (PRDFs) were calculated to assess the atomic structure. First-neighbour Ge–Ge correlation peaks were found at 2.53 Å (10% Ge), 2.63 Å (20%, 30%), 2.48 Å (40%), and 2.53 Å (50%), with a lack of well-defined second or third peaks, suggesting that the Ge NCQDs were predominantly amorphous under the simulated conditions. This is consistent with the limited timescales of MD simulations, which constrain the development of long-range crystalline order. The average radii of Ge NCQDs were estimated as 0.68 nm, 0.89 nm, and 1.83 nm for the 10%, 20%, and 30% Ge models, respectively. These results indicate a direct scaling relationship between Ge content and NCQD size, providing a predictive framework for tuning QD dimensions *via* compositional control of the starting $Si_{1-x}Ge_xO_2$ alloy.

The MD simulations successfully predict general trends in QD formation behaviour, which were corroborated by experimental STEM and XRD analyses. For the quantitative QD formation modelling, an analytical model was derived to predict the radius of Ge NCQDs and the surrounding oxide thickness as functions of the Ge content in $Si_{1-x}Ge_xO_2$ alloys. This model captures the redistribution of mass and volume during high-temperature annealing and provides a scalable framework for composition-driven NCQD design.

Assuming that the annealing time is enough so that most of the Ge atoms agglomerate, the mass and density relationships before and after annealing can be found. Besides, this assumption seems effective in most of the cases since we observed that 80–90% of the agglomeration was completed within 5–15 minutes of RTA. When the final NCQD radius is R and the tunnelling oxide thickness is d, which is equally distributed at the top and bottom of the NCQD, the initial volume of the SiGeO layer, V_{initial}, and the final volume, V_{final}, of Ge QD and the surrounding SiO_2 can be expressed in the following equations:

$$V_{\text{initial}} = \frac{N(1-x)m_{\text{Si}} + Nxm_{\text{Ge}} + 2Nm_{\text{O}}}{x\rho_{\text{GeO}_2} + (1-x)\rho_{\text{SiO}_2}} = t^3 \quad (1)$$

$$V_{\text{final}} = \frac{Nxm_{\text{Ge}}}{\rho_{\text{Ge}}} + \frac{N(1-x)m_{\text{Si}} + 2N(1-x)m_{\text{O}}}{\rho_{\text{SiO}_2}} = t'^3 \quad (2)$$

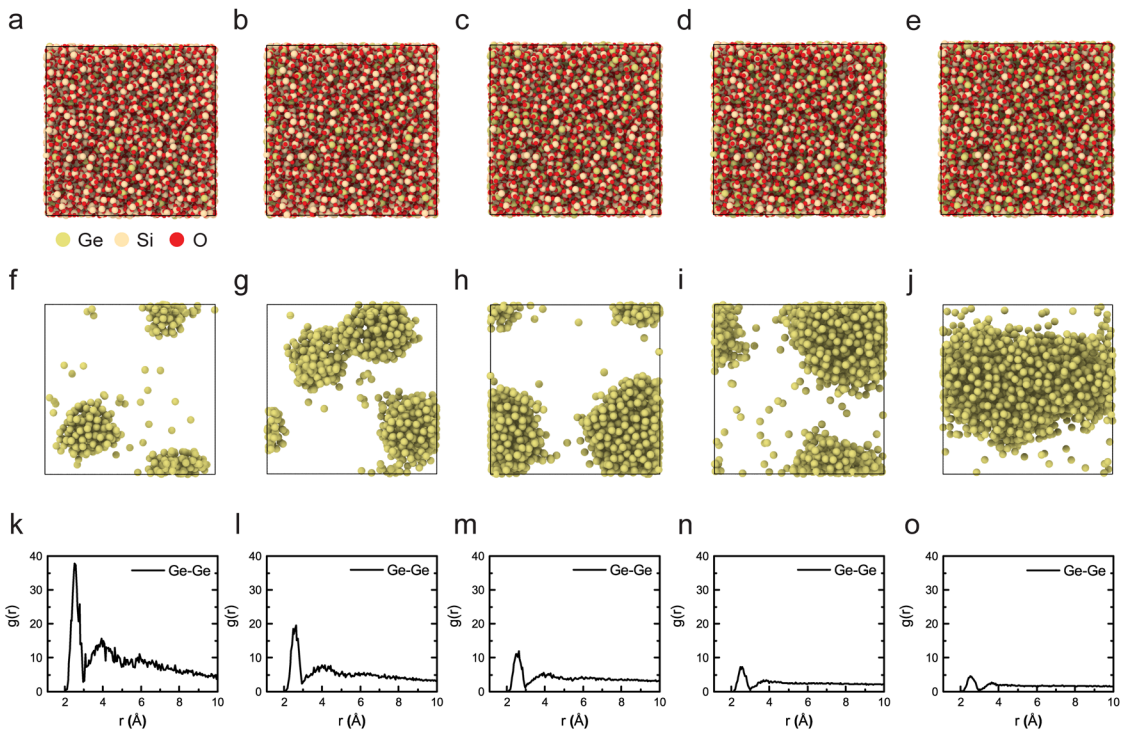

Fig. 6 Schematic illustrations for the Ge nanoparticle formation during the annealing process at 3000 K: (a–e) initial structures and (f–j) final structures after 100 ns of the $Si_{0.9}Ge_{0.1}O_2$, $Si_{0.8}Ge_{0.2}O_2$, $Si_{0.7}Ge_{0.3}O_2$, $Si_{0.6}Ge_{0.4}O_2$, and $Si_{0.5}Ge_{0.5}O_2$ alloys. (k–o) PRDF graphs of Ge–Ge bonds investigated from the simulation results of the $Si_{0.9}Ge_{0.1}O_2$, $Si_{0.8}Ge_{0.2}O_2$, $Si_{0.7}Ge_{0.3}O_2$, $Si_{0.6}Ge_{0.4}O_2$, and $Si_{0.5}Ge_{0.5}O_2$ alloys.

$$R = \left[\frac{3Nm_{Ge}x}{4\pi\rho_{Ge}}\right]^{1/3} \quad (3)$$

$$d = \tfrac{1}{2}\sqrt[1/3]{t'} - R \quad (4)$$

Here, t and t' represent the cube lengths of the oxide before and after annealing, which are derived from the density difference between the GeO_x and Ge QDs. N is the total number of Si and Ge atoms, while x is the Ge content of $Si_{1-x}Ge_xO_2$ alloys. m and ρ are the atomic masses and material densities, respectively. Consequently, the tunnelling oxide thickness, d, can be determined using the final volume and the QD radius from eqn (2) and (3), and expressed in eqn (4).

Model predictions were validated against MD simulations and the experimental results. The analytical model yielded results closely matching the MD data (Table 2). The slight discrepancy in QD radius (~0.25 nm) is attributed to the overestimation of Ge density in the MD simulation, likely due to the limited relaxation time following high-temperature annealing.

The oxide length ratio α, defined as t'/t, depends only on the Ge content, x, and remains independent of system size. This parameter captures the volumetric shrinkage resulting from the densification and crystallization of Ge within the oxide. As x increases, the difference in oxide lengths becomes more pronounced. In Fig. 7, the MD data yielded results closely matching the analytical model with the slight underestimation in α, indicating that model predictions were validated against MD simulations for a 10–35% Ge alloy. For x = 0.3 in Fig. 6(h), the theoretical value of α was calculated to be 0.928, while the MD simulation yielded a slightly lower value of 0.887 due to the relatively small QD radius. When x = 0.2, the calculated ratio was 0.952 from the equations.

In experimental measurement in Fig. 7, the samples prepared by double-step annealing were closely fitted with the analytical model prediction. During oxidation, the $Si_{0.5}Ge_{0.5}$ substrate forms a SiGeO alloy containing ~20% of Ge content. The Ge NCQD sample in Fig. 6 exhibits a slight overestimation of α (~0.045) and an underestimation of R (~0.13) as the Ge QDs were not fully crystallized and contained regions with GeO_x boundaries. Consequently, the ratio increased to 0.997. Nevertheless, the enhanced Ge agglomeration achieved by double-step annealing ensures that the overall trend in both oxide length ratio and QD radius was consistent with the model's predictions.

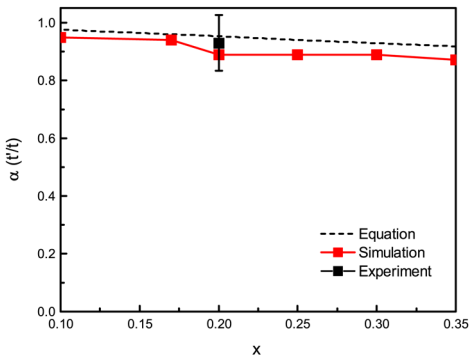

Fig. 7 Comparison of the oxide length ratios (α) obtained from simulations and experiments compared with the calculations from eqn (2)–(4). x represents the Ge content relative to Si in the SiGeO alloy. For the experimental results, the error bar denotes the standard deviation (±0.1).

The combination of MD simulations and experimental validation demonstrates that Ge NCQDs can be reliably synthesized within a SiO_x matrix from our method. The MD simulations provide valuable insights into the agglomeration dynamics of Ge atoms, predicting the QDs' sizes with different Ge contents. Experimental results corroborate these findings, showing that Ge NCQDs through the self-assembly method exhibit crystalline properties under optimized annealing conditions. Furthermore, the analytical model provides a reliable first-order tool for predicting both the QD size and surrounding oxide thickness as functions of initial alloy composition and processing. This modelling approach enables rational design of Ge QD-based structures with tailored geometry for quantum confinement and efficient charge transfer. It serves as a valuable foundation for implementing predictive control in quantum nanomaterial synthesis and device integration.

Table 2 Comparison of the MD simulation results with values calculated from eqn (2)–(4) for the size of Ge QDs after the annealing process. All samples were subsequently relaxed at 300 K

x	Methods	α (t'/t)	R (nm)	d (nm)
0.10	Equation	0.976	1.04	1.19
	Simulation	0.947	0.68	0.49
0.17	Equation	0.960	1.56	1.23
	Simulation	0.938	1.33	1.39
0.20	Equation	0.951	1.17	0.79
	Simulation	0.888	0.88	0.95
0.25	Equation	0.940	1.79	0.96
	Simulation	0.889	1.60	1.00
0.30	Equation	0.928	1.88	0.82
	Simulation	0.887	1.75	0.83
0.35	Equation	0.916	2.01	0.70
	Simulation	0.870	1.70	0.88

3 Conclusions

In this study, a deterministic and thermodynamically guided synthesis strategy was developed to form spatially confined Ge NCQDs within a silicon oxide matrix, enabling precise control over dot size and oxide thickness. By combining MD simulations, analytical modelling, and experimental validation, we demonstrated that the size and distribution of Ge QDs can be predictively tuned through the Ge content and thermal processing conditions, providing a CMOS-compatible pathway for engineering quantum-confined structures.

The double-step annealing process enabled the formation of spatially confined, single-row Ge NCQDs with a size of 9.2 nm, separated from the SiGe channel by oxide barriers as thin as 3.2 nm. Moreover, PL measurements confirmed size-dependent emission in the visible range, highlighting quantum confinement effects at room temperature. This work lays the foundation for materials-driven control of QD geome-

tries, enabling a reproducible route toward next-generation QD technologies.

Author contributions

S. H. P.: conceptualization, methodology, investigation, software, data analysis, visualization, and writing – original draft. G. M. S.: conceptualization, methodology, investigation, data analysis, and visualization. J. W. K.: investigation, data analysis, and visualization. Y. H. L.: investigation, data analysis, and visualization. G. L.: methodology, visualization, and investigation. H. J. L.: methodology and investigation. B. D. K.: conceptualization, methodology, supervision, resources, project administration, and funding acquisition. All authors: writing – review & editing.

Conflicts of interest

There are no conflicts to declare.

Data availability

The data, including the MD simulations of amorphous SiO_2 and GeO_2 formation, experiments on the temperature-dependent oxidation behaviour of SiGe, and additional PL measurements of Ge QDs that support the findings of this study, are available in the supplementary information (SI) and from the corresponding author upon reasonable request.

Supplementary information is available. See DOI: https://doi.org/10.1039/d5nr04252f.

Acknowledgements

This work was supported by the 'Samsung Research Funding and Incubation Center' of Samsung Electronics (SRFC-IT2102-01) and the National Research Foundation (NRF) grant funded by the Korean Government (Ministry of Science and ICT) (No. RS-2025-16069611).

References

1 D. S. Kumar, B. J. Kumar and H. Mahesh, Quantum nanostructures (QDs): an overview, in *Synthesis of inorganic nanomaterials*, 2018, pp. 59–88.
2 L. E. Brus, Electron–electron and electron–hole interactions in small semiconductor crystallites: The size dependence of the lowest excited electronic state, *J. Chem. Phys.*, 1984, **80**, 4403–4409.
3 K. K. Likharev, Single-electron devices and their applications, *Proc. IEEE*, 1999, **87**, 606–632.
4 S. Krishnamurthy, *et al.*, PbS/CdS quantum dot room-temperature single-emitter spectroscopy reaches the telecom O and S bands via an engineered stability, *ACS Nano*, 2020, **15**, 575–587.
5 W. Heiss, *et al.*, Highly luminescent nanocrystal quantum dots fabricated by lattice-type mismatched epitaxy, *Phys. E*, 2006, **35**, 241–245.
6 M. Aouassa, *et al.*, Growth and characterization of SiGe/SiO_2 core/shell nanocrystals on insulators, *ACS Appl. Electron. Mater.*, 2024, **6**, 4120–4129.
7 M. Aouassa, *et al.*, Growth of Ge QDs-decorated SiGe nanocrystals: toward integration of quantum dots and Mie resonators in ultrathin film for photodetection and energy harvesting, *ACS Appl. Electron. Mater.*, 2024, **6**, 3290–3296.
8 M. A. Alenizi, *et al.*, Electrical and dielectric characterization of Ge quantum dots embedded in MIS structure (AuPd/SiO_2: Ge QDs/n-Si) grown by MBE, *Phys. B*, 2024, **685**, 415962.
9 T. C. Chen, L. S. Lee, W. Z. Lai and C. W. Liu, The characteristic of HfO_2 on strained SiGe, *Mater. Sci. Semicond. Process.*, 2005, **8**, 209–213.
10 E. Long, A. Galeckas and A. Y. Kuznetsov, Ge concentrations in pile-up layers of sub-100 nm SiGe films for nano-structuring by thermal oxidation, *J. Vac. Sci. Technol., B:Nanotechnol. Microelectron.:Mater., Process., Meas., Phenom.*, 2012, **30**, 041212.
11 M. Kanoun, *et al.*, Electronic properties of Ge nanocrystals for nonvolatile memory applications, *Solid-State Electron.*, 2006, **50**, 1310–1314.
12 C. H. Kao, C. S. Lai, C. S. Huang and K. M. Fan, Ge nanocrystal charge trapping devices fabricated by one-step oxidation on poly-SiGe, *Appl. Surf. Sci.*, 2008, **255**, 2512–2516.
13 W. K. Chim, Germanium Nanocrystal Non-Volatile Memory: Fabrication, Charge Storage Mechanism and Characterization, *Nanoscale*, 2025, **14**, 4195.
14 B. H. Koh, *et al.*, Traps in germanium nanocrystal memory and effect on charge retention: Modeling and experimental measurements, *J. Appl. Phys.*, 2005, **97**, 124305.
15 E. W. H. Kan, *et al.*, Effect of annealing profile on defect annihilation, crystallinity and size distribution of germanium nanodots in silicon oxide matrix, *Appl. Phys. Lett.*, 2003, **83**, 2058–2060.
16 W. R. Chen, T. C. Chang, Y. T. Hsieh, S. M. Sze and C. Y. Chang, Formation of Ge nanocrystals using $Si_{1.33}Ge_{0.67}O_2$ and $Si_{2.67}Ge_{1.33}N_2$ film for nonvolatile memory application, *Appl. Phys. Lett.*, 2007, **91**, 102106.
17 M. Yang, *et al.*, Effect of annealing on charge transfer in Ge nanocrystal based nonvolatile memory structure, *J. Appl. Phys.*, 2009, **106**, 103701.
18 J. P. Zhao, *et al.*, Amorphous Ge quantum dots embedded in SiO_2 formed by low energy ion implantation, *J. Appl. Phys.*, 2008, **103**, 124304.
19 J. H. Wu and P. W. Li, Ge nanocrystals MOS capacitors with Ge nanocrystals formed by oxidation of poly-Si0.88Ge0.12, *Semicond. Sci. Technol.*, 2006, **22**, S89–S92.
20 C. H. Kao, C. S. Lai, M. C. Tsai, C. H. Lee, C. S. Huang and C. R. Chen, Using thermal oxidation and rapid thermal

annealing on polycrystalline-SiGe for Ge nanocrystals, *Mater. Res. Soc. Symp. Proc.*, 2007, **1071**, 10710321.
21 C. H. Kao, C. S. Lai, C. S. Huang and K. M. Fan, Ge nanocrystal charge trapping devices fabricated by one-step oxidation on poly-SiGe, *Appl. Surf. Sci.*, 2008, **255**, 2512–2516.
22 A. Rodríguez, *et al.*, Ge nanocrystals embedded in a SiO_2 matrix obtained from SiGeO films deposited by LPCVD, *Semicond. Sci. Technol.*, 2010, **25**, 045032.
23 J. D. Cox, D. D. Wagman and V. A. Medvedev, *CODATA key values for thermodynamics*, Hemisphere Publishing Corp., New York, 1989.
24 D. C. Paine, C. Caragianis and A. F. Schwartzman, Oxidation of $Si_{1-x}Ge_x$ alloys at atmospheric and elevated pressure, *J. Appl. Phys.*, 1991, **70**, 5076–5084.
25 M. A. Nicolet and W. S. Liu, Oxidation of GeSi, *Microelectron. Eng.*, 1995, **28**, 185–191.
26 M. I. Richard, *et al.*, Tracking defect type and strain relaxation in patterned Ge/Si(001) islands by X-ray forbidden reflection analysis, *Phys. Rev. B:Condens. Matter Mater. Phys.*, 2011, **84**, 075314.
27 Q. Zheng, *et al.*, Unveiling the complexity of nanodiamond structures, *Proc. Natl. Acad. Sci. U. S. A.*, 2023, **120**, e2301981120.
28 Y. Maeda, Visible photoluminescence from nanocrystallite Ge embedded in a glassy SiO_2 matrix: evidence in support of the quantum-confinement mechanism, *Phys. Rev. B: Condens. Matter Mater. Phys.*, 1995, **51**, 1658–1670.
29 Y. Maeda, N. Tsukamoto, Y. Yazawa, Y. Kanemitsu and Y. Masumoto, Visible photoluminescence of Ge microcrystals embedded in SiO_2 glassy matrices, *Appl. Phys. Lett.*, 1991, **59**, 3168–3170.
30 K. Surana, P. K. Singh, H. W. Rhee and B. Bhattacharya, Synthesis, characterization and application of CdSe quantum dots, *J. Ind. Eng. Chem.*, 2014, **20**, 4188–4193.
31 P. H. Liao, *et al.*, Size-tunable strain engineering in Ge nanocrystals embedded within SiO_2 and Si_3N_4, *Appl. Phys. Lett.*, 2014, **105**, 172106.
32 A. P. Thompson, *et al.*, LAMMPS-a flexible simulation tool for particle-based materials modeling at the atomic, meso, and continuum scales, *Comput. Phys. Commun.*, 2022, **271**, 108171.
33 J. K. Bording, Molecular-dynamics simulation of Ge rapidly cooled from the molten state into the amorphous state, *Phys. Rev. B:Condens. Matter Mater. Phys.*, 2000, **62**, 7103–7109.